N K-edge x-ray-absorption study of heteroepitaxial GaN films

M. Katsikini
Department of Physics, Aristotle University of Thessaloniki, 54006 Thessaloniki, Greece and Hahn-Meitner Institute (A.S.), Glienicker Strasse 100, D-14109 Berlin, Germany

E. C. Paloura
Department of Physics, Aristotle University of Thessaloniki, 54006 Thessaloniki, Greece

M. Fieber-Erdmann
Hahn-Meitner Institute (A.S.), Glienicker Strasse 100, D-14109 Berlin, Germany

J. Kalomiros
Department of Physics, Aristotle University of Thessaloniki, 54006 Thessaloniki, Greece

T. D. Moustakas
College of Engineering, Boston University, Boston, Massachusetts 02215

H. Amano and I. Akasaki
Department of Electrical and Electronic Engineering, Meijo University, Nagoya 468, Japan
(Received 10 February 1997; revised manuscript received 14 August 1997)

The microstructure of GaN films grown by electron cyclotron resonance (ECR) molecular-beam epitaxy (MBE) and hydride vapor-phase epitaxy (HVPE) is studied using x-ray-absorption measurements at the N K edge. The local microstructure around the N atom is found to be distorted. The nearest neighbors of the N atom are four Ga atoms, N_1 of which are located at a distance $R_1 = 1.95$ Å, which is expected, and N_2 at a distance $R_2 = R_1 + 0.25$ Å. This distortion is more pronounced in the cubic ECR-MBE and the HVPE hexagonal samples where the ratio N_2/N_1 is equal to 1. In the rest of the samples the distortion is smaller and the ratio N_2/N_1 takes the value 0.33. Nitrogen deficiency is not detected in the second nearest-neighbor shell and the N atoms are found at the expected distance of 3.11 Å. [S0163-1829(97)04144-1]

I. INTRODUCTION

Gallium nitride (GaN) is a wide-band-gap semiconductor that finds applications in uv and visible light emitters and detectors as well as in optical data storage devices.[1,2] In addition to its wide-band gap, GaN has other attractive properties such as good thermal and chemical stability and physical hardness,[3] which render it suitable for a wide range of microelectronics applications. Recently, the alloys of GaN with other III-V nitrides (AlN and InN) have attracted a great deal of interest because they permit band-gap engineering.

GaN exists in two polytypes: the hexagonal (wurtzite structure, α-GaN) and the thermodynamically metastable cubic (zinc-blende structure, β-GaN). The hexagonal and the cubic structures of the GaN polytypes are nearly identical when viewed along the (0001) and the (111) directions, respectively. Since the formation of stacking faults is energetically favorable, phase stabilization of the cubic polytype is difficult and growth of mixed-phase crystals is often observed.[3] The structure and the quality of heteroepitaxially grown GaN crystals depend on the growth conditions, the substrate, and its preparation, and the use of a buffer layer. However, despite the progress in GaN growth, a variety of extended or point defects are incorporated in the GaN films due to the large lattice mismatch of GaN with the available substrates, the small reactivity of N with Ga, and the large differences in the thermal expansion coefficients of the substrate and the epitaxial film.[4,5] According to recent theoretical studies of native defects in GaN,[6–8] the formation energy of nitrogen vacancies V_N is very low and therefore V_N are present in all the GaN films. Other native defects with relatively low formation energies that can exist in GaN are N antisites, Ga vacancies, and the interstitial N defect. The presence of native defects such as antisites or Ga interstitials induces strain that cannot be easily and totally relieved by distortion of the microstructure around the defect. The origin of this strain is the large difference between the covalent radii of Ga and N (1.26 and 0.75 Å, respectively). Another characteristic of GaN is the strong ionic character of the N-Ga bond.[9]

The lattice parameters of epitaxially grown GaN films can be affected by a number of factors such as thermal strain, free-electron concentration, and extended or point defects, e.g., N vacancies (V_N) and Ga antisite defects (Ga_N). It was shown that the volume of the unit cell decreases (a and c decrease) if the concentration of V_N in the films is high.[10] According to Lagerstedt and Monemar,[11] the decrease of the lattice parameters of GaN due to the presence of V_N could be approximated by $\Delta a/a \sim \Delta c/c \sim -V_N/N_{GaN}$. In addition to that, the lattice constants depend on the presence of dopants and on the growth rate and can be deformed by thermal strain. GaN films grown on Si or Al_2O_3 are subjected to

0163-1829/97/56(20)/13380(7)/$10.00 © 1997 The American Physical Society

TABLE I. Growth conditions and information about the GaN samples under study.

Sample name	Growth technique	T_{growth} (°C)	Substrate	Symmetry	Thickness (μm)
GaN57	ECR MBE	600	p-Si(001)	cubic	1.60
GaN67	ECR MBE	600	n-Si(111)	mixed	0.80
GaN179	ECR MBE	600	Al_2O_3(0001)	hexagonal	1.67
GaN*A*4	HVPE	1030	Al_2O_3(0001)	hexagonal	10.0

tensile or compressive stress upon cooling from the growth temperature. Biaxial stress causes a volume-conserving distortion of the unit cell and can be relaxed via formation of microcracks.[12]

Extended x-ray-absorption fine-structure (EXAFS) spectroscopy is a nondestructive characterization technique that probes the local microstructure around a central absorbing atom. An EXAFS spectrum, which extends from 50 up to 1000 eV above the absorption edge, shows the dependence of the absorption coefficient (x-ray-absorption cross section) on the incident x-ray beam energy above the absorption edge. From an EXAFS spectrum the type of the neighbors, the coordination number, the distance between the central and the neighboring atoms, and the Debye-Waller factors can be found.[13] In addition to that, the bond angles can be determined from angular-dependent measurements.[14] In the solid state the absorption coefficient shows an oscillatory behavior above the absorption edge because the outgoing photoelectron wave interferes with the backscattered wave from the neighboring atoms. These EXAFS oscillations can be clearly seen after the subtraction of the atomic absorption, i.e., the absorption of the central atom in the absence of neighboring atoms. The oscillatory part $\chi(k)$ of the EXAFS spectrum after background subtraction and normalization with the structureless background is given by the equation

$$\chi(k)=\sum_j A_j(k)\sin[2kr_j+\theta_{ij}(k)], \qquad (1a)$$

where

$$A_j(k)=N_jS_j(k)F_j(k)\exp(-2\sigma_j^2k^2)\exp\left(\frac{-2r_j}{\lambda_j(k)}\right)\frac{1}{kr_j^2}, \qquad (1b)$$

$\varphi_{ij}(k)$ is the total phase shift, which contains contributions from both the absorber and the backscatterer and affects the origin of the sine wave and its frequency; N_j is the number of atoms in the nearest-neighbor (NN) shell; $S_i(k)$ is an amplitude reduction factor due to shake-up–shake-off processes originating from multiple excitations of the passive electrons in the excited/absorbing atom; $F_j(k)$ is the backscattering amplitude of the atoms in the NN shell; and $\sigma_j(k)$ is the Debye-Waller factor (relative displacement of the neighboring atom along the bond direction), which accounts for static and thermal disorder. The factor $e^{-2r_i/\lambda_j(k)}$ describes the inelastic losses [$\lambda_j(k)$ is the mean free path of the photoelectron].[17] EXAFS can be applied in both crystalline and amorphous materials and it can be also applied to detect local lattice distortions.[15,16] The common detection schemes in the soft x-ray range are the total electron yield (TEY) and fluorescence yield (FLY) modes. The TEY mode is surface sensitive and meticulous surface preparation and cleaning are required in order to avoid contributions from surface contaminants. The FLY mode is bulk sensitive and is thus better suited when the bulk material properties are sought. The fluorescence yield spectra can suffer from self-absorption effects that affect mostly the amplitude of the EXAFS spectrum and thus the calculated coordination numbers and the Debye-Waller factors. The distortion of the spectra due to self-absorption depends on the geometry of the experiment, i.e., the angle of incidence, and are strong in thick or concentrated samples.[17]

Perlin *et al.*[18] have previously reported on EXAFS measurements at the Ga *K* edge of GaN. Their EXAFS measurements were conducted under high-pressure conditions (up to 48 GPa) for the identification of the high-pressure phase transition. The spectra were recorded over an energy range of 400 eV and the authors reported on the pressure-induced changes in the second NN shell (Ga-Ga distances). Some of us have previously reported on the N *K*-edge near-edge x-ray-absorption fine-structure (NEXAFS) measurements of GaN.[19] We have demonstrated that NEXAFS is an identifying characteristic of the cubic and hexagonal symmetries and can be used for the determination of the fractions of the cubic and hexagonal polytypes in mixed-phase samples.

Here we present EXAFS characterization results on GaN at the N *K* edge. The films were grown heteroepitaxially and our results demonstrate that the microstructure around the N atom is distorted.

II. EXPERIMENTAL DETAILS

The samples used for the present study are labeled GaN57, GaN67, GaN179, and GaN*A*4. The samples GaN57, GaN67, and GaN179 were grown with electron cyclotron resonance (ECR) molecular-beam epitaxy (MBE) using ammonia as the nitrogen source. The sample GaN*A*4 was grown with hydride vapor-phase epitaxy (HVPE) using a Ga solid source, HCl, and ammonia (NH_3). The growth conditions and selected film properties are listed in Table I, while details on growth and their properties have been reported previously.[12,20–23] Angular-dependent N *K*-edge NEXAFS measurements reported recently[20] revealed that GaN57 and GaN179 are pure cubic and hexagonal samples, respectively. GaN67 is a mixed-phase sample with 25% of the material in the cubic and 75% in the hexagonal phase, respectively.[20] The sample GaNA4 is also in the hexagonal phase.[24]

The EXAFS and NEXAFS measurements were conducted using the monochromator SX-700-I at the electron storage

ring BESSY in Berlin. This monochromator has high resolution and flux in the soft-x-ray region (200–2000 eV) and is thus ideally suited for measurements at the N *K* edge.[25] The spectra were recorded with a step of 2 eV in the energy range 370–1100 eV and the data acquisition time was 1 s per point. The ECR-MBE samples were measured at the N *K* edge at room temperature (300 K). The spectra of the HVPE sample were recorded at 300 and 160 K. The angle of incidence was 55° and the detection angle was 35° (measured relative to the sample surface). The spectra were recorded in the fluorescence yield mode using a high-purity Ge detector positioned along the electric field vector (the resolution of the detector at the N *K* edge was about 100 eV). Due to the high-absorption cross section of air in the soft-x-ray region, the experiment was performed in an ultrahigh vacuum (UHV) chamber with a base pressure $\leqslant 7\times 10^{-10}$ mbar. In order to improve the signal-to-noise ratio more than 20 spectra were collected and averaged for each sample at each experimental condition. The EXAFS spectra were normalized to the primary photon flux by division with the total electron yield spectra from a clean (non-absorbing) Si wafer, which yields a good measure of the monochromator transmission function over the range of interest (370–1100 eV). The clean Si surface was prepared by etching in buffered HF and annealing under UHV conditions at 850°–900 °C for a few minutes.

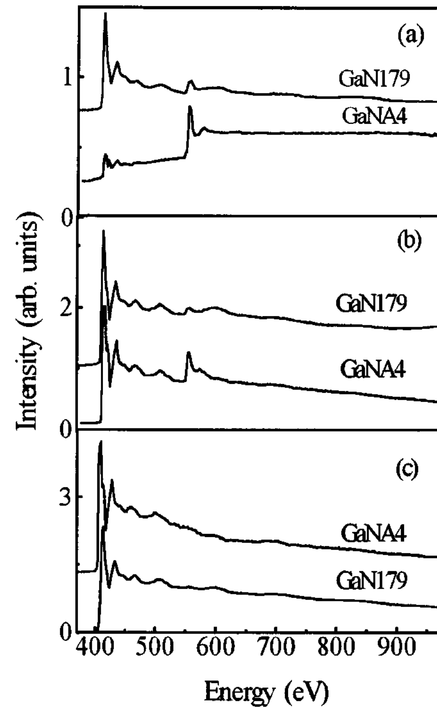

FIG. 1. N *K*-edge EXAFS spectra from the hexagonal samples GaN*A*4 and GaN179 recorded in the TEY and the FLY detection modes. All the spectra are normalized with the clean Si spectrum: (a) the as-recorded TEY spectra, (b) the as-recorded FLY spectra, and (c) the FLY spectra after the subtraction of the oxygen contribution (the spectra are shifted relative to each other along the *y* axis).

III. RESULTS AND DISCUSSION

The as-recorded TEY and FLY spectra from the hexagonal samples GaN*A*4 and GaN179, normalized with the clean Si spectrum, are shown in Figs. 1(a) and 1(b), respectively. The signal due to surface and bulk oxygen is detected at about 540 eV and is strong enough to interfere with the signal from the N *K* edge. Among the examined samples GaN*A*4 contains the highest concentration of bulk oxygen. The oxygen concentration in GaN*A*4 is about 6 at. %, as estimated from the edge jump heights of the two edges and the fluorescence yields of O and N. Due to the presence of the bulk oxygen, the TEY spectra cannot be analyzed. In addition to the presence of oxygen, the TEY spectra are distorted due to charging effects that are energy and time dependent and are clearly seen in the TEY spectrum from the film GaN*A*4 [Fig. 1(a)]. Given that, in the FLY detection mode the electronic separation of the oxygen signal is possible[26] and since we are interested in the bulk film properties, the results presented here are based on the FLY spectra. In the case of the ECR-MBE samples, which did not contain significant oxygen contamination, only one window for the N signal was used and the signal due to oxygen was easily eliminated by adjustment of the width of the detection window. The FLY spectra after the electronic elimination of the oxygen signal and normalization with the clean Si spectrum are shown in Fig. 1(c).

A. Fitting procedure

Equation (1), which describes the EXAFS oscillations, can be used as cited in the case of amorphous and cubic samples. In the case of crystalline solids with lower than cubic symmetry or adsorbed molecules on surfaces, polarization effects should be taken into account. For linearly polarized light (synchrotron radiation light is linearly polarized parallel to the ring plane) the amplitude A_j of the wave scattered from the ith NN shell depends on the angle between the electric-field vector of the incident beam and the vector between the central atom and the jth atom of the ith NN shell. In the case of higher than twofold symmetry around the surface normal there is a value for the angle of incidence (relative to the sample surface) called the ''magic angle,''[27] which in the case of α-GaN is equal to 54.7°. For this value of the angle of incidence polarization effects are null and the coordination numbers found from the EXAFS analysis do not need any corrections. Our spectra were recorded at an angle of incidence $\theta = 55°$, which is, within the experimental error, equal to the magic angle.

As mentioned in the Introduction, the FLY spectra should be checked for self-absorption effects.[26] More specifically, if the thickness of the sample is much higher than the $1/\mu_{\mathrm{tot}}$, where μ_{tot} is the total absorption cross section, and the concentration of the central-absorbing atom is high, then self-absorption corrections should be included in the calculation.[26,28] The μ_{tot} at the absorption edge is found about 10^5 cm^{-1} and $1/\mu_{\mathrm{tot}}$ is 10^{-5} cm or 0.1 μm. The thicknesses of all the examined films are 10–100 times larger than 0.1 μm and therefore self-absorption corrections are probably needed. Following the procedure proposed by Tröger *et al.*,[26] self-absorption corrections (SAC's) have been calculated (the information depth at the N *K* edge is found to be about 0.05 μm). The corrections were done directly in the *k*

TABLE II. Two models that have been used for the fitting. R is the distance from the central atom, N is the coordination number, and T is the type of neighboring atom. The lattice constants and the structure of each polytype are also listed.

Polytype		α-GaN			β-GaN	
Structure		hexagonal (C_{6v})			cubic (T_d)	
Lattice constants		$a=3.19$ Å, $c=5.189$ Å			$a=4.50$ Å	
Fitting models	T	R	N	T	R	N
	Ga	1.949	3	Ga	1.949	4
	Ga	1.959	1			
	N	3.182	6	N	3.182	12
	N	3.190	6			
	Ga	3.233	1	Ga	3.731	12
	Ga	3.738	3			
	Ga	3.742	6			

space [$\chi(k)$ spectra], where $k=\sqrt{2m(E-E_0)/\hbar^2}$, m is the electron mass, and E_0 is the absorption threshold, which was defined as the maximum of the first derivative of the EXAFS spectrum (roughly the absorption K-edge energy position). The experimental $\chi(k)$, $\chi_{\text{expt}}(k)$, was multiplied by a factor $1/[1-S(k)]$, where $S(k)=\mu_0(E)/[\mu_{\text{tot}}(E)+\mu_{\text{tot}}(E_f)g]$; $\mu_0(E)$ is the absorption cross section of the absorbing N atom, $\mu_{\text{tot}}(E)$ is the total absorption cross section (with contributions from both N and Ga atoms), E_f is the N K_a fluorescence radiation (390 eV), and g is a geometric factor, which, in the present case, is equal to $\tan(55°)=1.428$. For the calculation of $S(k)$ we used the values of the absorption cross sections (in barns) published by Yeh and Lindau.[29] Using the formula

$$\mu(\text{cm}^{-1})=\mu\left(\frac{\text{b}}{\text{atom}}\right)\frac{\rho}{1.66M}\left(\frac{\text{g}}{\text{cm}^3}\right),$$

where M is the atomic mass of the element and ρ is the density of GaN, the absorption cross sections were transformed in cm^{-1} ($\rho_{\text{GaN}}=6.095$ g/cm^3).[30]

After normalization of the spectra by division with the spectrum from the clean Si wafer the atomic absorption background was subtracted using the AUTOBK program. Then the spectra were fitted using models constructed with the program FEFF6.[31] FEFF calculates the "paths" corresponding to the NN shells for an ideal structure. Each path contains information about the neighboring atoms such as the energy threshold, the NN distance, the mean free path of the photoelectron, the effective amplitude, and the phase of the backscattering function (curved wave corrections are included).[31] The two models used for the fitting of the N K-edge spectra are shown in Table II. The $k^3\chi(k)$ spectra were fitted using the program FEFFIT3.23.[31] Only single-scattering paths were taken into account because the contribution of multiple scattering proved to be insignificant. The amplitude reduction factor $S_j(k)$, which is characteristic of the absorbing atom, was kept constant in all the examined samples to the value of 0.93. An additional energy shift ΔE_0 was added in the theoretical path in order to match with the experimental spectrum. ΔE_0 was kept constant and equal to 3.74 eV for the N K-edge spectra. The fixed values of ΔE_0 and $S_j(k)$ were determined after a series of fitting of all the examined spectra and they were kept the same for all the NN shells. The value of λ was the same as the theoretically calculated. The initial values for R_i and N_i were those predicted from the model, while the initial values for the Debye-Waller (DW) factors (A_i) were calculated using the correlated Debye model.[32] Iterations were done for R_i, N_i, and A_i.

B. N K-edge results

The N K-edge spectra were fitted in the k range 4–11 Å^{-1} and in the r range 1–5 Å. The rather high value of k_{min} was used in order to accommodate for the nonlinear backscattering amplitude of Ga, which has two maxima and a dip at about 3 Å^{-1}, as shown in Fig. 2. Oxygen paths have not been included in the analysis of the spectra recorded at the N K edge because the amount of oxygen is small and the backscattering amplitude of O is very similar to that of N, as shown in Fig. 2.

As discussed in Sec. II, the spectra should be checked for SAC's. The $S(k)$ and the $1/[1-S(k)]$, in the k range 3–11 Å^{-1}, are shown in Figs. 3(a) and 3(b), respectively. It is apparent that for the N K-edge measurements at an angle of incidence equal to 55°, the SAC's are not significant. That is more clearly seen in Fig. 4(a), where the as-recorded $\chi_{\text{expt}}(k)$ of the 10-μm-thick sample GaN$A4$ (thick line) along with the self-absorption (SA) -corrected spectrum (thin line) $\chi_{\text{cor}}(k)$ are shown. The corresponding Fourier transform (FT) is shown in Fig. 4(b). The small SA effect is probably due to the high-absorption cross section of Ga in the energy range 300–1000 eV [$\mu_{\text{Ga}}(450\text{ eV})\approx 2\mu_{\text{N}}(450\text{ eV})$]. The N_i

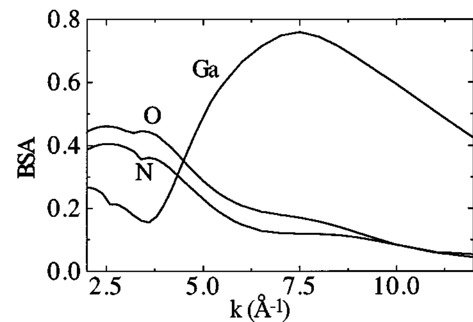

FIG. 2. Amplitude of the backscattering functions (BSA) of Ga, N, and O calculated with the FEFF6.01 code.

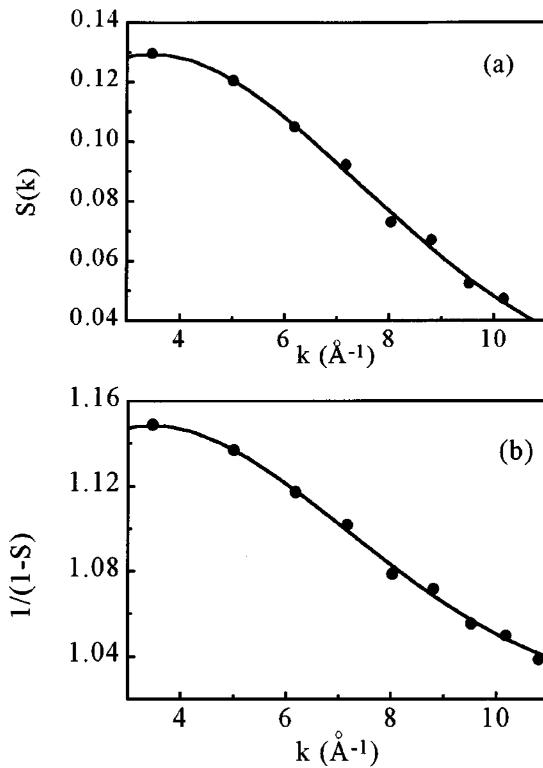

FIG. 3. Self-absorption correction factor: (a) $S(k)$ and (b) $1/[1-S(k)]$.

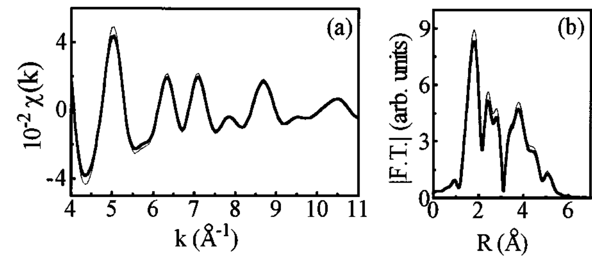

FIG. 4. (a) The $k^3\chi(k)-k$ spectrum from the 10-μm-thick GaNA4 sample and (b) the corresponding FT. The as-recorded and SA-corrected spectra are shown as solid and dotted lines, respectively.

and σ_i determined from the as-measured and SA-corrected spectra are different only by 10%, i.e., the correction is equal to or smaller than the error bar. Despite the small values of the SAC's, the reported results in Table III are based on the SAC spectra.

The k^3-weighted $\chi(k)$ spectra of all the examined samples are shown in Fig. 5 and the corresponding FT's are shown in Fig. 6. The experimental curves and the fitting are shown in thick and thin solid lines, respectively. The spectra from GaN67 and GaNA4 are Fourier filtered in the range 1.1–5.2 Å. As shown in Fig. 6, the FT of the experimental spectrum at the first peak splits in two, as indicated by the arrow. This splitting is not predicted in the FEFF6 model. To obtain a good fitting of the experimental $k^3\chi(k)$ curve, one more N-Ga path at a distance $R_2=R_1+0.25$ Å, in addition to the expected N-Ga path at $R_1=1.94$ Å, is included. Fourier filtering of the split peak (1.2–2.5 Å) reveals that the envelope function is similar to that corresponding to the first Ga path. An additional Ga path is thus indicated. The results of the EXAFS analysis for the three NN shells are listed in Table III. The distortion in the N-Ga distance is observed in both the first NN shell and the next Ga shell where the Ga atoms are found at distances 3.7 and 4.1 Å. However, Table III contains results only from the first three NN shells since the error in the determination of R_i and N_i for the shells at distances larger than 3 Å is higher because the shells are not well separated. A distortion in the N-N distances, similar to that found in the N-Ga distances, is not detected, possibly due to the small backscattering amplitude of N. The errors listed in Table III were determined after background subtraction with two different spline functions and using the same DW factors for the fitting (the errors due to the fitting procedure are much smaller than the errors due to background subtraction).

The value of R_1 in the two first N-Ga shells is found to be smaller in GaN179 and GaN67 than in GaN57 and GaNA4. In GaN57 and GaNA4, R_1 is found to be equal to 1.95 Å at both 160 and 300 K, while in GaN67 and GaN179 the distance R_1 is equal to 1.91 Å. Using the published value of $a=4.50$ Å (Refs. 21–24) for the cubic sample GaN57, the theoretically predicted value of R_1 is 1.95 Å, i.e., in very-

TABLE III. Results of EXAFS analysis. The first and second NN shells consist of Ga atoms, while the third consists of N atoms. N_i, R_i, and A_i $(i=1,\ldots,3)$ stand for the coordination number, neighbor distance, and Debye-Weller factor, respectively. The amplitude reduction factor is 0.93.

Fitting parameters	GaN57	GaNA4 (300 K)	GaNA4 (160 K)	GaN67	GaN179
$N_1\pm10\%$	2.08	2.13	2.27	2.90	2.90
$R_1\pm0.01$ Å	1.95	1.96	1.95	1.91	1.91
$A_1\pm10\%$ (Å^2)	5.6×10^{-3}	6.0×10^{-3}	6.4×10^{-3}	5.2×10^{-3}	5.6×10^{-3}
$N_2\pm10\%$	1.91	1.86	1.72	1.10	1.10
$R_2\pm0.01$ Å	2.18	2.18	2.19	2.19	2.19
$A_2\pm10\%$ (Å^2)	5.9×10^{-3}	6.3×10^{-3}	6.7×10^{-3}	5.5×10^{-3}	5.9×10^{-3}
$N_3\pm15\%$	13.00	11.00	11.00	13.00	13.00
$R_3\pm0.03$ Å	3.08	3.07	3.09	3.13	3.12
$A_3\pm15\%$ (Å^2)	1.0×10^{-2}	9.2×10^{-3}	7.6×10^{-3}	1.1×10^{-2}	1.1×10^{-2}

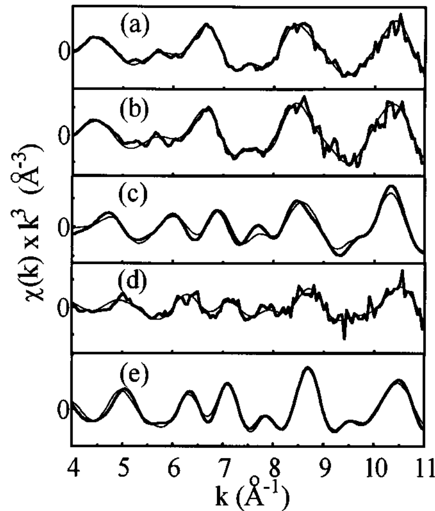

FIG. 5. N K-edge $k^3\chi(k)$ spectra versus k for (a) GaN179, (b) GaN67, (c) GaN57, (d) GaNA4 at 300 K, and (e) GaNA4 at 160 K. The recorded spectrum and the fitting are shown as thick and thin lines, respectively.

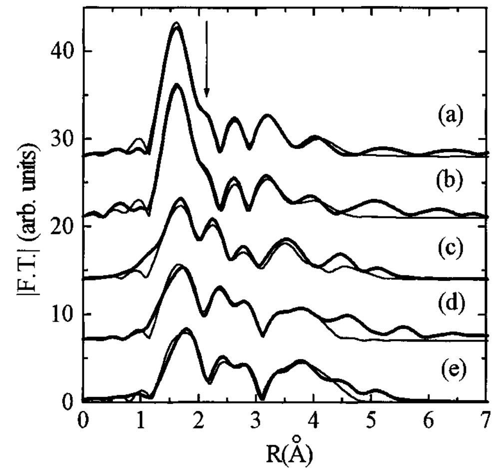

FIG. 6. Fourier transform of the spectra shown in Fig. 5 for (a) GaN179, (b) GaN67, (c) GaN57, (d) GaNA4 at 300 K, and (e) GaNA4 at 160 K. The recorded spectrum and the fitting are shown as thick and thin lines, respectively. The distortion of the NN distances is indicated by the arrow.

good agreement with the EXAFS results. In order to accommodate the smaller value of R_1 measured in GaN67 and GaN179, the value of c should be smaller than that in GaNA4 and GaN57 by 2% (assuming that the whole unit cell is smaller). Here it should be pointed out that a distortion of the lattice parameters can depend on the substrate, the growth conditions, the thickness of the film, the presence of contamination (e.g., oxygen), and the presence of defects such as dislocations and micro- or macrocracks[12] or native defects.[11]

The central N atom is fourfold coordinated with N_1 Ga atoms at a distance R_1 and N_2 atoms at R_2, while $N_1+N_2=4$. The N_2/N_1 ratio, which can be considered as a measure of the distortion in the first NN shell, takes the value $N_2/N_1=1$ in GaN57 and GaNA4, while in GaN67 and GaN179 it is equal to $N_2/N_1=0.33$. This distortion could be an indication of distorted tetrahedra in the bulk of the material. However, due to the large excitation volume that contributes to the EXAFS signal, the N_2/N_1 ratio contains also information from distorted regions at the grain boundaries. The distortion in the N-Ga distance is ''universal'' since it is observed in samples with different symmetry (α-, β-, and mixed-phase GaN) and grown with different techniques. This distortion could be attributed to the thermal strain and/or inhomogeneous strain. It should be mentioned that in AlN, which also belongs in the family of the III-V nitrides, such a distortion was not detected.[33]

The third NN shell consisting of N atoms is found at the expected distance of 3.12 ± 0.05 Å with the expected coordination number of 12 ± 1 N atoms. Therefore, N deficiency is not detected, at least within the $\pm15\%$ accuracy of EXAFS in the determination of the coordination number in the N shell.

IV. CONCLUSION

The EXAFS measurements at the N K edge reveal that the local microstructure around the N atom is distorted due to the existence of two different N-Ga distances R_1 and R_2, where $R_2=R_1+0.25$ Å. This distortion is detected in all the examined samples, despite the differences in the growth method, chemical stoichiometry, and structural perfection. Possible origins of the distortion are the inhomogeneous strain due to point and extended defects[34] (dislocations, grain boundaries, and micro- or macrocracks) and thermal strain due to the large differences in the thermal expansion coefficients of GaN and the substrates. The distortion in the NN shell is important because it alters the interatomic energies and the overlapping of the atomic potentials and thus affects the band structure and the energy of the valence-band maximum[35,36] as well as the performance of devices based on GaN and its alloys with other III-V nitrides.[36,37] The different degree of distortion, expressed by the ratio N_2/N_1, could be related to the differences in the structural defects among the examined samples. For example, GaN57 is reported to be highly faulted[22] with an average grain size of the order of 500 Å, while the grain size in GaN179 and GaN67 is 1500 Å. Distortion due to biaxial stress depends on the elastic constants of GaN and leads to changes in the bond lengths and angles.[38,39] Such a deviation of the value of the N-Ga distance from the expected value of 1.95 Å is identified in the films GaN179 and GaN67, where $R_1=1.91$ Å.

Our measurements do not detect N deficiency, at least within the experimental error of EXAFS ($\pm15\%$ of the coordination number N_3). Due to the large difference in the backscattering amplitudes of the Ga and N atoms and the differences in their FLY's a more accurate identification of a possible N deficiency (in stoichiometric films such as those studied here) using EXAFS will be difficult.

ACKNOWLEDGMENT

This work was realized with partial financial support from the EC-HCM program (Grant No. CHGE-CT93-0027).

[1] S. D. Lester, F. A. Ponce, M. G. Craford, and D. A. Steigerwald, Appl. Phys. Lett. **66**, 1250 (1995).

[2] H. Sakai, T. Koide, H. Suzuki, M. Yamaguchi, S. Yamasaki, M. Koike, H. Amano, and I. Akasaki, Jpn. J. Appl. Phys., Part 2 **34**, L1429 (1995).

[3] *Properties of Group III Nitrides*, edited by J. H. Edgar (INSPEC, Exeter, 1994).

[4] T. Kozawa, T. Kachi, H. Kans, H. Nagase, N. Koide, and K. Manabe, J. Appl. Phys. **77**, 4389 (1995).

[5] W. Lei and W.-X. Ni, Appl. Phys. Lett. **68**, 705 (1996).

[6] Jörg Neugebauer and Chris G. Van de Walle, Phys. Rev. B **50**, 8067 (1994).

[7] P. Boguslawski, E. L. Briggs, and J. Bernholc, Phys. Rev. B **51**, 17 255 (1995).

[8] I. Corczyca, A. Svane, and N. E. Christensen, Solid State Commun. **101**, 747 (1997).

[9] K. Miwa and A. Fukumoto, Phys. Rev. B **48**, 7897 (1993).

[10] M. Leszczynski, H. Teisseyre, T. Suski, I. Grzegory, M. Bockowski, J. Jun, S. Porowski, K. Pakula, J. M. Baranowski, C. T. Foxon, and T. S. Cheng, Appl. Phys. Lett. **69**, 73 (1996).

[11] O. Lagerstedt and B. Monemar, Phys. Rev. B **19**, 3064 (1979).

[12] K. Hiramatsu, T. Detchprohm, and I. Akasaki, Jpn. J. Appl. Phys., Part 1 **32**, 1528 (1993).

[13] Boon K. Teo, *EXAFS; Basic Principles and Data Analysis* (Springer-Verlag, Berlin, 1986).

[14] D. Konigsberger and R. Prins, *X-Ray Absorption: Principles, Techniques and Applications of EXAFS and XANES* (Wiley, New York, 1988).

[15] U. Scheuer and B. Lengerer, Phys. Rev. B **44**, 9883 (1991).

[16] N. Papanikolaou, R. Zeller, P. H. Dederichs, and N. Stefanou, Phys. Rev. B **55**, 4157 (1997).

[17] L. Tröger, D. Arvanitis, K. Baberschke, H. Michaelis, U. Grimm, and E. Zschech, Phys. Rev. B **46**, 3283 (1992).

[18] P. Perlin, C. Jauberthie-Carillon, J. P. Itie, A. San Miguel, I. Grzegory, and A. Polian, Phys. Rev. B **45**, 83 (1992).

[19] M. Katsikini, E. C. Paloura, and T. D. Moustakas, Appl. Phys. Lett. **69**, 4206 (1996).

[20] T. D. Moustakas, T. Lei, and R. J. Molnar, Physica B **185**, 36 (1993).

[21] T. Lei, T. D. Moustakas, R. J. Graham, Y. He, and S. J. Berkowitz, J. Appl. Phys. **71**, 4933 (1992).

[22] S. N. Basu, T. Lei, and T. D. Moustakas, J. Mater. Res. **9**, 2370 (1994).

[23] T. Lei, K. F. Ludwig, and T. D. Moustakas, J. Appl. Phys. **74**, 4430 (1993).

[24] M. Katsikini and E. C. Paloura (unpublished).

[25] H. Petersen, Nucl. Instrum. Methods Phys. Res. A **246**, 260 (1986).

[26] L. Tröger, D. Arvanitis, H. Rabus, L. Wenzel, and K. Baberschke, Phys. Rev. B **41**, 7297 (1990); L. Tröger, T. Yokoyama, D. Arvanitis, T. Lederer, M. Tischer, and K. Baberschke, *ibid.* **49**, 888 (1994), and references therein.

[27] J. Stöhr, *NEXAFS Spectroscopy* (Springer-Verlag, Berlin, 1992).

[28] *Handbook on Synchrotron Radiation*, edited by E. E. Koch (North-Holland, Amsterdam, 1983).

[29] J. J. Yeh and I. Lindau, At. Data Nucl. Data Tables **32**, 1 (1985).

[30] D. Bimberg, R. Blachnik, M. Carolone, P. J. Dean, Th. Grave, G. Harbeke, K. Hübner, U. Kaufmann, W. Kress, O. Madelung, W. von Münch, U. Rössler, J. Schneider, M. Schulz, and M. S. Skolnick, in *Zahlenwerte und Funktionen aus Naturwissenschaft und Technik*, edited by O. Madelung, M. Schulz, and H. Weiss, Landolt-Börnstein, New Series, Group III, Pt. 17 (Springer-Verlag, Berlin, 1982).

[31] J. Mustre de Leon, J. J. Rehr, R. C. Albers, and S. I. Zabinsky, Phys. Rev. B **44**, 3937 (1992).

[32] E. Sevillano, H. Meuth, and J. J. Rehr, Phys. Rev. B **20**, 4908 (1979).

[33] M. Katsikini, E. C. Paloura, T. Cheng, and C. T. Foxon, J. Appl. Phys. **82**, 1166 (1997).

[34] M. Leszczynski, H. Teisseyre, T. Suski, I. Grzegory, M. Bockowski, J. Jun, S. Porowski, K. Pakula, J. M. Baranowski, C. T. Foxon, and T. S. Cheng, Appl. Phys. Lett. **69**, 73 (1996).

[35] Y. M. Sirenko, J.-B. Jeon, K. W. Kim, M. A. Littlejohn, and M. A. Stroscio, Appl. Phys. Lett. **69**, 2504 (1996).

[36] J. Xie, J. Zi, and K. Zhang, Phys. Status Solidi B **192**, 95 (1995).

[37] S. Kamiyama, K. Ohnaka, M. Suzuki, and T. Uenoyama, Jpn. J. Appl. Phys., Part 2 **34**, L821 (1995).

[38] M. Nido, Jpn. J. Appl. Phys., Part 2 **34**, L1513 (1995).

[39] K. Kim, W. R. Lambrecht, and B. Segal, Phys. Rev. B **50**, 1502 (1994).